

Resolving the $^{11}\text{B}(p, \alpha_0)$ Cross Section Discrepancies between 0.5 and 3.5 MeV

Michael Munch¹ and Oliver Sølund Kirsebom¹ and Jacobus Andreas Swartz^{1a} and Hans Otto Uldall Fynbo¹

Department of Physics and Astronomy, Aarhus University, Ny Munkegade 120, 8000 Aarhus C, Denmark

Received: date / Revised version: date

Abstract. The reaction $^{11}\text{B}(p, 3\alpha)$ is relevant for fields as diverse as material science, nuclear structure, nuclear astrophysics, and fusion science. However, for the channel proceeding via the ground state of ^8Be , the available cross-section data shows large discrepancies of both normalization and energy scale. The present paper reports on a measurement of the $^{11}\text{B}(p, \alpha_0)$ cross section using an array of modern large area segmented silicon detectors and low beam current on an enriched thin target with the aim of resolving the discrepancies amongst previous measurements.

PACS. PACS-key describing text of that key – PACS-key describing text of that key

1 Introduction

The reaction $^{11}\text{B}(p, 3\alpha)$ is relevant for fields as diverse as material science, nuclear structure, nuclear astrophysics, and fusion science. In a sequential picture, this reaction can proceed via the ground state of ^8Be , $^{11}\text{B}(p, \alpha_0)^8\text{Be}$, or via the first excited state, $^{11}\text{B}(p, \alpha_1)^8\text{Be}^*$.

Boron depth profiling in bulk matter can be studied using the technique of nuclear reaction analysis (NRA) where a nuclear reaction on the element of interest produces a particle with high enough energy to escape the material, and the energy distribution of the emitted particles can be used to deduce the depth profile. Boron depth profiling using NRA requires an accurate cross section of the $^{11}\text{B}(p, \alpha_0)$ reaction in the energy range up to 3–4 MeV [1].

The rate of the $^{11}\text{B}(p, 3\alpha)$ reaction is also relevant for understanding the astrophysical abundances of the light elements Li, Be, and B [2,3]. Specifically, the abundances of these elements in stellar atmospheres can be depleted due to plasma mixing phenomena inside the stars at a rate which depends on fundamental nuclear cross sections.

The $^{11}\text{B}(p, 3\alpha)$ reaction is considered a candidate for fusion energy generators as an alternative to e.g. the most favored $t(d, n)\alpha$ reaction [4]. In order to evaluate the feasibility of the $^{11}\text{B}(p, 3\alpha)$ reaction accurate cross sections are required [5].

Finally, the cross section of the $^{11}\text{B}(p, 3\alpha)$ reaction provides a direct probe for resonances in ^{12}C above the $^{11}\text{B}+p$ threshold. For proton energies up to 2 MeV the excitation spectrum exhibits resonances due to three isospin $T = 1$

states at 16.11, 16.62 and 17.76 MeV, which have spin and parity of 2^+ , 2^- and 0^+ and whose properties are well established. Additionally, a very broad 1^- , $T = 1$ resonance and sub-threshold resonances of unknown spin and parity are believed to contribute to the excitation spectrum in the region between the 2^- and 0^+ resonances [6,7,8].

A handful of measurements over extended ranges of beam energies and/or emission angles of the final state particles have been published, but these measurements differ significantly both in the energy scale and in the absolute normalization of the cross sections. Figure 1 shows

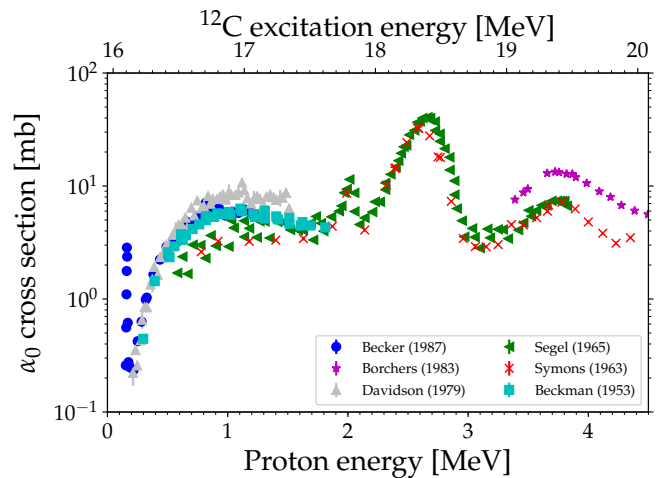


Fig. 1. Angle-integrated α_0 cross section as reported by Refs. [9,6,7,10,11,12] (tabulated data available via EXFOR [13]). Deviations both in the absolute normalization and energy calibration are evident.

Send offprint requests to: H. O. U. Fynbo (fynbo@phys.au.dk)

^a Present address: Center for Nuclear Technologies, Technical University of Denmark, Frederiksborgvej 399, 4000 Roskilde, Denmark

cross section data from a set of measurements of the $^{11}\text{B}(p, \alpha_0)$ target was oriented at angles of 0° and 180° with respect to the beam axis which is the focus of the present paper. As is evident, there are significant deviations of the order of 100 keV in the energy scale and up to 70 % in the magnitude of the cross section between different measurements. Likely sources of such deviations can be accelerator energy calibrations and inaccurate evaluations of target thicknesses.

Some of us have recently published a re-measurement of the $^{11}\text{B}(p, 3\alpha)$ reaction at a proton energy corresponding to the 16.11 MeV $2^+ T = 1$ resonance, which produced a more precise and accurate determination of the cross section at that energy [14]. Here we use the same experimental approach to study the $^{11}\text{B}(p, \alpha_0)$ reaction for proton energies in the range 0.5–3.5 MeV.

2 Experiment

The experiment was conducted at the Aarhus University 5 MeV accelerator which provided a beam of protons with an energy between 0.5 and 3.5 MeV. The beam impinged on a thin boron target which was oriented 45° with respect to the beam axis. The beam current was measured 1 m downstream of the target position and the beam spot was collimated to be $1\text{mm} \times 1\text{mm}$ by a set of horizontal and vertical slits.

The boron target was manufactured by evaporating 99 % enriched ^{11}B onto a thin $\sim 4\ \mu\text{g cm}^{-2}$ natural carbon backing. In order to determine the target thickness the

target was oriented at angles of 0° and 180° with respect to the beam axis and bombarded with 2 MeV α particles. The ^{11}B thickness could then be deduced from the energy shift of the carbon peak using the procedure described in Ref. [14]. The result was $12.6(12)\ \mu\text{g cm}^{-2}$.

Charged particles were detected using an array of four Double Sided Silicon Strip Detectors (DSSD) in close geometry. These provided a simultaneous detection of energy and position of emitted charged particles. The array consisted of two annular DSSDs (S3 from Micron Semiconductors) placed 42 mm up- and downstream of the target. Additionally, two quadratic DSSDs (W1 from Micron Semiconductors) were placed approximately 36 mm from the target center at an angles of 85° and 95° with respect to the beam axis.

The trigger logic was handled by a GSI VULOM4B module [15] running the TRLO II firmware [16]. The trigger logic was configured as a logical OR between all four detectors, with the downstream detector downscaled by a factor of eight. The firmware maintains scaler values for the accepted and total number of triggers for each detector. The deadtime for each run was determined from these.

The energy scan was performed in steps of 100 keV with smaller steps near well-known resonances. Data were acquired at each energy for approximately one hour with a beam current of 0.3–1 nA. Longer measurements were performed for the 0^+ state at 17.76 MeV and the 3^- state at 18.35 MeV. The result of these longer measurements will be reported separately [17].

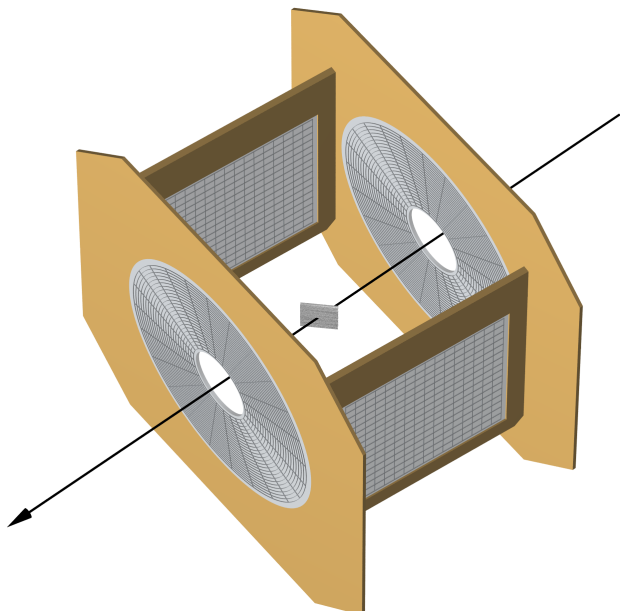


Fig. 2. Detection setup. Two annular detectors were placed 42 mm up- and downstream of the target, while two quadratic detectors were placed at 85° and 95° . The target was oriented 45° with respect to the beam axis, which is indicated by the arrow.

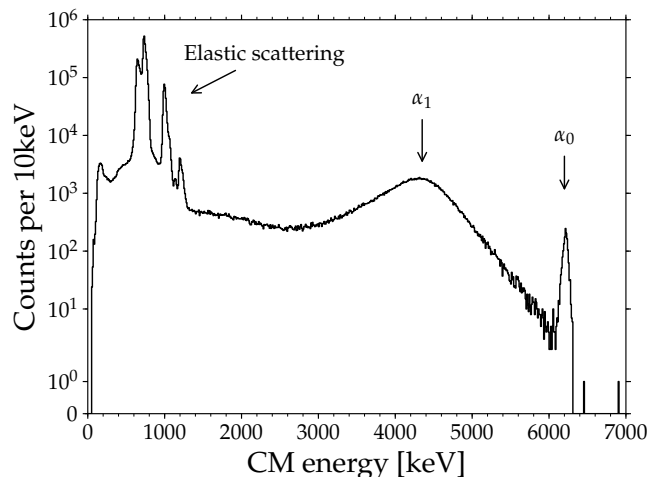


Fig. 3. Center-of-mass energy distribution for a proton energy of 800 keV. At high energy, one sees a sharp peak corresponding to α_0 . Below this peak is a broad distribution corresponding to reactions proceeding via the α_1 channel. Around 1 MeV there are various peaks corresponding to elastic proton scattering. The energy of the elastic protons might be larger than the beam energy since they have been corrected for α particle energy loss.

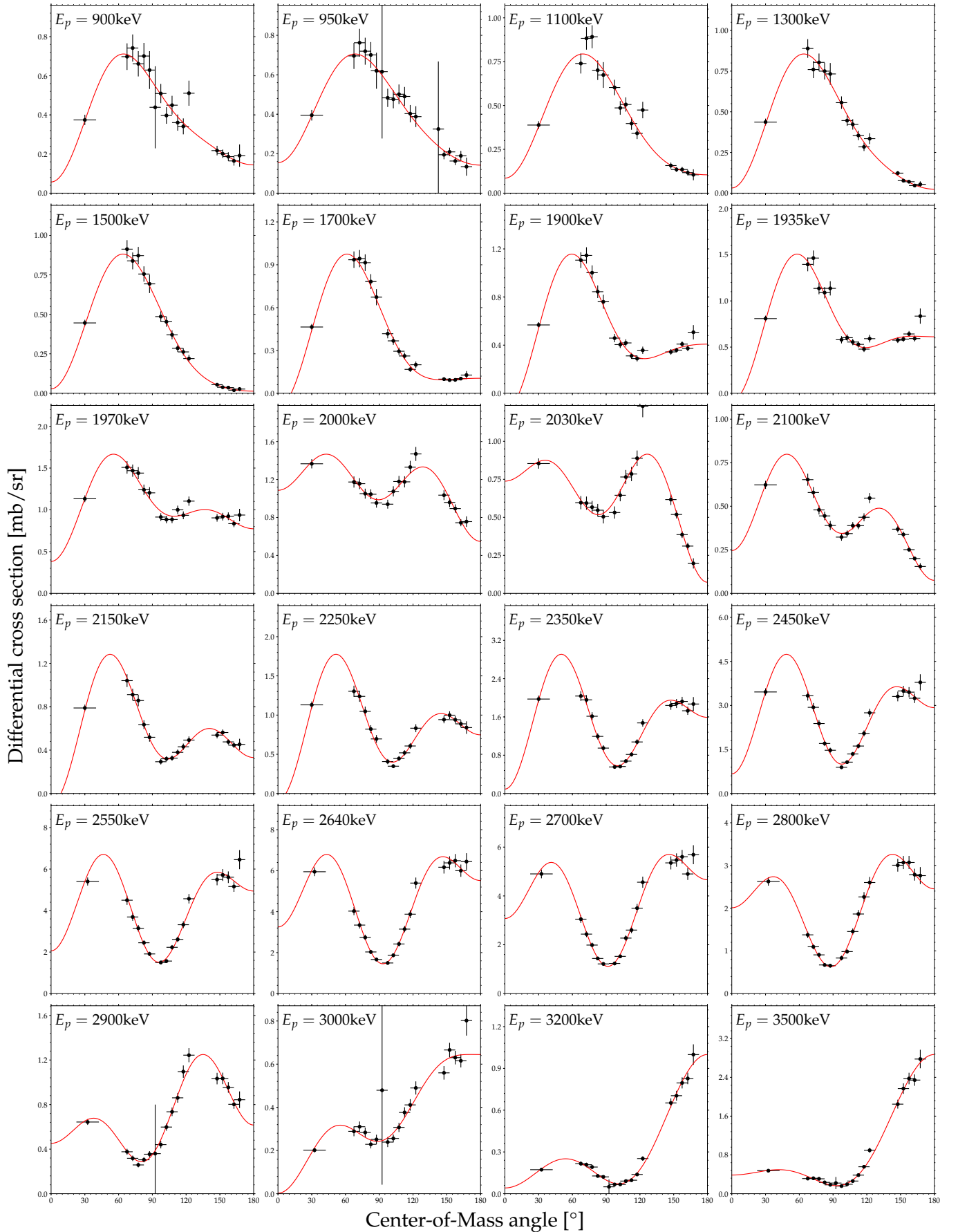


Fig. 4. Selection of angular distribution from 900 to 3500 keV. A slow evolution from slightly forward focussed below 2 MeV to approximately symmetric around 2.4 MeV to strongly backward focussed above 3 MeV.

3 Data reduction

The analysis was performed event by event on list-mode type data. The detected particles were assumed to be α particles and the energies were corrected for losses in the target foil and the dead layers of the detectors, which are ~ 500 nm thick for the annular design and ~ 100 nm for the quadratic design. The corrected energies and the angles were transformed to the beam-target center-of-mass (CM) system. An example of the resulting CM energy spectrum can be seen in fig. 3 with a clear peak at high energy corresponding to the α_0 channel. At lower energies the broad distribution corresponding to α_1 and its secondary particles is present. Peaks from the elastic scattering of the proton beam off boron, carbon, and small impurities of an element close to iron can also be seen at

low energies. To select the α_0 channel, a cut is placed on the α_0 peak and the CM angles projected out. A selection of the resulting angular distribution can be seen in fig. 4. The distributions evolve slowly from forward focussed to approximately symmetric to strongly backward focussed. During the analysis, it was observed that some pixels in the forward detectors were partially shadowed by the target ladder. Conservatively these pixels were excluded from the analysis and simulation.

In order to determine the solid angle of the detection system, a Monte Carlo simulation was performed with the SimX tool [19]. A beam of protons with a $1\text{mm} \times 1\text{mm}$ profile was generated and propagated to a random depth in the boron layer. At this location, an α_0 was generated and emitted isotropically in the CM system. The α_0 was propagated out of the target and into the detectors in a straight-line trajectory. Energy losses were calculated using the SRIM tables which approximately account for straggling [20]. The structure of the simulation output was identical to the real data and the simulated data was subjected to the same analysis as the real data. The solid angle for a given CM angle can then be calculated as the ratio between the number of detected hits to the number of simulated events. The angular distribution is then given by the ratio of the data and simulation for each CM angle. The differential cross section was in this way determined by scaling the angular distribution with the integrated current and acquisition deadtime. The resulting angular resolved cross sections were then fitted with

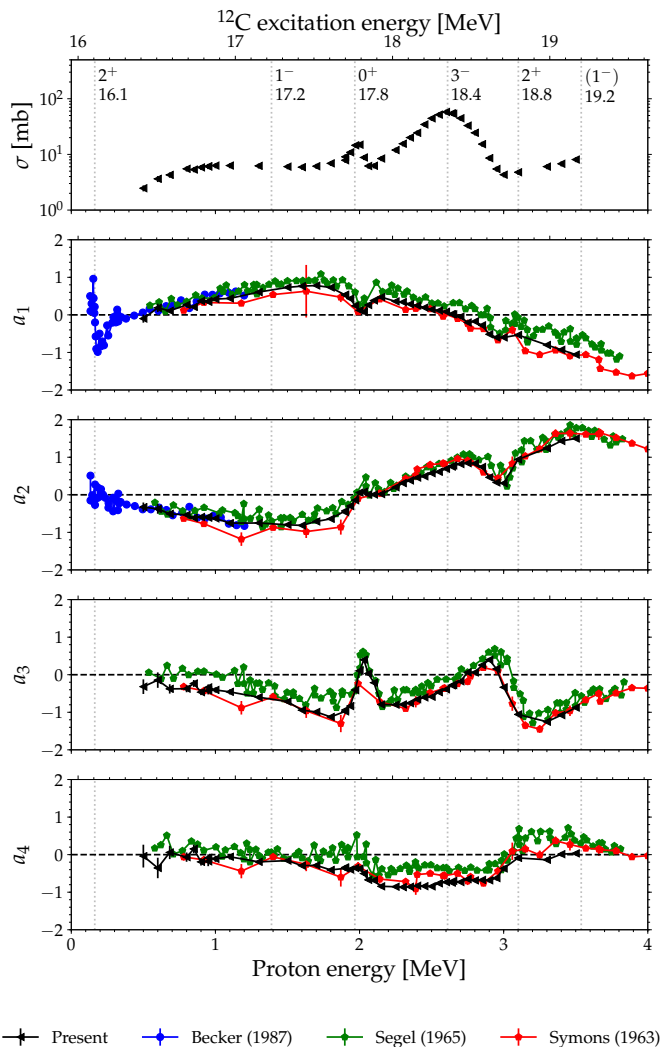


Fig. 5. Angle-integrated cross section and Legendre coefficients shown as a function of beam energy together with the coefficients obtained by Refs. [6, 7, 12]. The dashed vertical lines indicate the position of natural parity states in ^{12}C as listed in Ref. [18].

Table 1. Tabulated angle-integrated cross sections. The uncertainty is approximately 10% for all data points except the lowest two where it is 12%.

| E_p [keV] | $\sigma_{\alpha 0}$ [mb] | E_p [keV] | $\sigma_{\alpha 0}$ [mb] |
|-------------|--------------------------|-------------|--------------------------|
| 500 | 2.5(3) | 2150 | 8.4(9) |
| 600 | 3.6(4) | 2250 | 12.0(12) |
| 683 | 4.3(5) | 2300 | 15.5(16) |
| 800 | 5.5(6) | 2350 | 20(2) |
| 850 | 5.3(6) | 2400 | 24(2) |
| 900 | 5.8(6) | 2450 | 35(3) |
| 950 | 6.1(6) | 2500 | 44(4) |
| 950 | 6.1(6) | 2550 | 52(5) |
| 1000 | 6.3(6) | 2600 | 58(6) |
| 1100 | 6.3(6) | 2640 | 55(6) |
| 1300 | 6.2(6) | 2650 | 54(5) |
| 1500 | 6.0(6) | 2700 | 45(5) |
| 1600 | 5.9(6) | 2750 | 33(3) |
| 1700 | 6.1(6) | 2800 | 24(2) |
| 1800 | 6.9(7) | 2850 | 15.3(15) |
| 1900 | 7.9(8) | 2900 | 8.6(9) |
| 1900 | 9.1(9) | 2950 | 5.5(6) |
| 1935 | 10.9(11) | 3000 | 4.3(4) |
| 1970 | 14.6(15) | 3100 | 4.8(5) |
| 2000 | 14.9(15) | 3300 | 6.0(6) |
| 2030 | 8.8(9) | 3400 | 6.8(7) |
| 2060 | 6.2(6) | 3500 | 8.1(8) |
| 2100 | 6.3(6) | | |

the lowest five Legendre polynomials

$$\frac{d\sigma}{d\Omega}(\theta) = \frac{\sigma}{4\pi} \left[1 + \sum_{i=1}^4 a_i P_i(\cos \theta) \right]. \quad (1)$$

4 Results and discussion

The Legendre coefficients as a function of beam energy are shown in the lower four panels of fig. 5 together with the coefficients obtained by Refs. [6,7,12]. In addition, the position of the natural parity states, listed in the latest compilation [18], are also indicated. For the two lowest-order terms, there is generally good agreement between all four datasets in the regions of overlap. For the third-order term, there is excellent agreement between the present

data and Symons *et al.* (SY) while the agreement with Segel *et al.* (SE) is good above ~ 1.5 MeV, and a systematic deviation is observed below that energy. This deviation might be due to the experimental difficulties noted by SE for measurements below 1 MeV beam energy. For the fourth-order term, there is again good agreement with SY, but a systematic shift is seen at all energies when comparing to SE. We speculate that this is due to the latter only measuring at six different angles whereas SY measured either 8 or 13 angles. From the data, it appears that the 0^+ , 3^- and 2^+ levels have an appreciable effect on the Legendre coefficients, while the effect of the 1^- levels appear negligible. This might simply be due to their width being as large as ~ 1 MeV. With the present agreement with previous datasets, we are unable to discern between the two differing interpretations presented in Refs. [8,6,7] for the region below 2 MeV. The reader is thus referred to them for a detailed discussion of the angular coefficients.

The angle-integrated cross section can be seen in the first panel of fig. 5 and in tabular form in table 1. It shows the same behavior as observed in the previous measurements. In fig. 6 we compare data from the present experiment and the recent high-resolution differential cross section dataset of Kokkoris *et al.* (KO) for $\theta = 150^\circ$ [1]. The agreement is better than 5 keV which validates the overall energy calibration of the present dataset. A similar comparison shows good agreement between the present data and that of SY. Thus, we cannot verify the claim of KO of a discrepancy between the energy scales of KO and SY. However, the agreement between our data and those of SE requires the energy of SE to be shifted down by approximately 38 keV.

As discussed in the introduction, there are several normalization issues between the different datasets [9,6,7,10,11,12]. In order to shed light on this, the ratios between the cross sections of other datasets and the present have been computed. This can be seen in fig. 7 where the me-

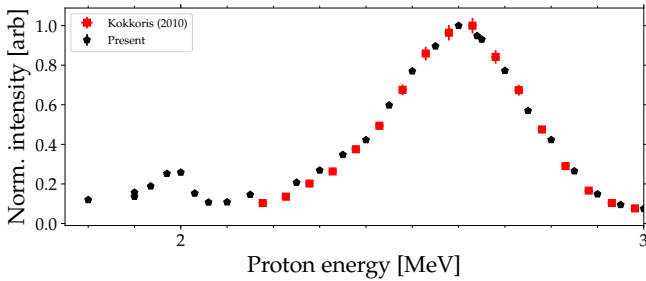


Fig. 6. Comparison of the present data and the recent high-resolution dataset by Kokkoris *et al.* (KO) for $\theta = 150^\circ$ [1]. Each dataset has been normalized so the maximum value is 1. The energy scale of the two dataset agrees better than 5 keV.

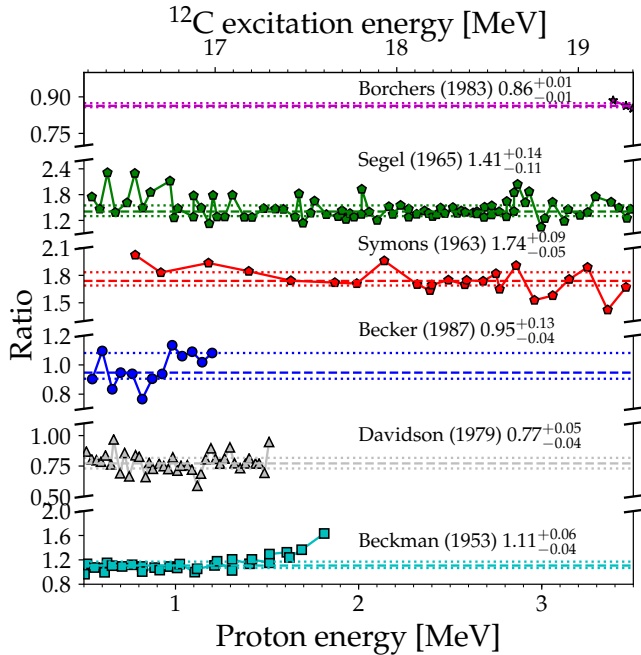


Fig. 7. Ratio of datasets [9,6,7,10,11,12] to a linear interpolation of the present dataset. The dashed line indicates the median, while the two dotted lines indicate the 25 and 75 percentiles. See the text for details.

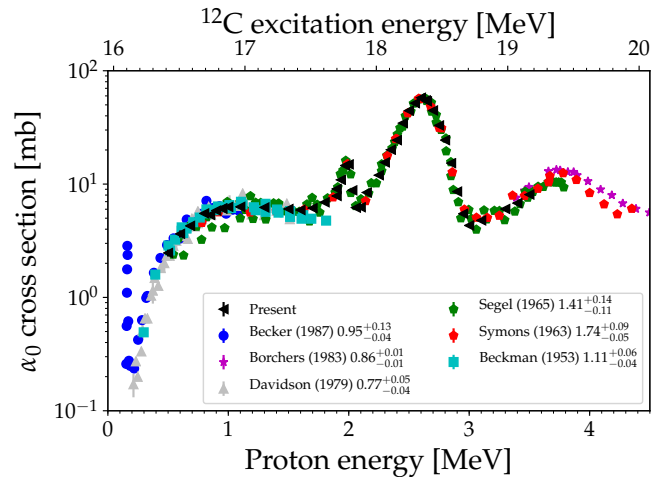


Fig. 8. Adjusted α_0 cross section (tabulated data available via EXFOR [13]). All datasets except BE and BO have been scaled by their median ratio to the present dataset.

dian ratio and the 25–75 inter quartile ratio are written in the legend. Note that the spectrum of SE has been shifted in energy as discussed above. The first conclusion is that within error the present measurement is consistent with the measurement of Becker *et al.* (BE), while the difference compared to Davidson *et al.* is a constant scaling factor. There also seems to be simple scaling relations for the data of Beckman *et al.* below ~ 1.3 MeV and the data of SE and SY in the range 1.5–2.75 MeV, while larger deviations occur outside these ranges. The present data only overlaps with the energy range measured by Borchers *et al.* (BO) in a limited range. However, within that range, the agreement is better than 2σ .

Scaling all datasets except BE and BO with constant factors given in fig. 7 yields the cross sections seen in fig. 8, which confirms visually that the different data sets can be brought into agreement by a constant scaling. Considering the good agreement between our measurement and the two most recent experiments by BE and BO, we argue that the overall normalization is now better than 15 %.

5 Conclusion

We have measured the $^{11}\text{B}(p, \alpha_0)$ reaction for proton energies in the range 0.5–3.5 MeV. From an analysis of the angular distributions, total cross sections and energy dependent Legendre polynomial coefficients have been extracted from the data. Disagreements between previous measurements [9, 6, 7, 10, 11, 12] on both the magnitude and energy dependence of the cross section have been resolved.

There is disagreement in the literature on the interpretation of the cross section and Legendre coefficients below 2 MeV in terms of resonances in ^{12}C . Symons *et al.* interprets this as ghosts of resonances below the proton threshold with spin and parity 2^+ or 3^- [6], while Barker interprets this region as a broad 1^- resonance in addition to the high energy tail of a broad 0^+ resonance below the proton threshold in ^{12}C [8].

We were unable to resolve this issue with a measurement of the α_0 channel. Instead this issue requires a measurement of the α_1 channel and probably also of the phase-space (Dalitz) distributions of the 3α emission of that channel. That will provide additional information on the spin and parity of the involved resonances in ^{12}C , which should be fed into a new R-matrix analysis similar to that performed by Barker.

Acknowledgement

We would like to thank Folmer Lyckegaard for manufacturing the target. We also acknowledge financial support from the European Research Council under ERC starting grant LOBENA, No. 307447. OSK acknowledges support from the Villum Foundation through Project No. 10117. MM acknowledges support from the Nustar Colaboration.

References

1. M. Kokkoris, A. Kafkarkou, V. Paneta, R. Vlastou, P. Misaelides, A. Lagoyannis, Nuclear Instruments and Methods in Physics Research, Section B: Beam Interactions with Materials and Atoms **268**, 3539 (2010)
2. A.M. Boesgaard, C.P. Deliyannis, A. Steinhauer, The Astrophysical Journal **621**, 991 (2005)
3. L. Lamia, C. Spitaleri, V. Burjan, N. Carlin, S. Cherubini, V. Crucillà, M.G. Munhoz, M.G.D. Santo, M. Gulino, Z. Hons et al., Journal of Physics G: Nuclear and Particle Physics **39**, 015106 (2012)
4. D. Moreau, Nuclear Fusion **17**, 13 (1977)
5. M.H. Sikora, H.R. Weller, Journal of Fusion Energy **35**, 538 (2016)
6. G. Symons, P. Treacy, Nuclear Physics **46**, 93 (1963)
7. R.E. Segel, S.S. Hanna, R.G. Allas, Physical Review **139**, B818 (1965)
8. F.C. Barker, Nuclear Physics A **707**, 277 (2002)
9. O. Beckman, T. Huus, Č. Zupančič, Physical Review **91**, 606 (1953)
10. J.M. Davidson, H.L. Berg, M.M. Lowry, M.R. Dwarakanath, A.J. Sierk, P. Batay-Csorba, Nuclear Physics, Section A **315**, 253 (1979)
11. F. Borchers, H. De Jong, J. Krug, E. Kuhlmann, Nuclear Physics A **405**, 141 (1983)
12. H.W. Becker, C. Rolfs, H.P. Trautvetter, Zeitschrift für Physik A Atomic Nuclei **327**, 341 (1987)
13. N. Otuka, E. Dupont, V. Semkova, B. Pritychenko, A.I. Blokhin, M. Aikawa, S. Babykina, M. Bossant, G. Chen, S. Dunaeva et al., Nuclear Data Sheets **120**, 272 (2014)
14. M. Munch, H.O. Uldall Fynbo, The European Physical Journal A **54**, 138 (2018), 1805.10924
15. J. Hoffman, VULOM4b data sheet (2013), accessed: 2017-05-10, http://www.gsi.de/fileadmin/EE/Module/VULOM/vulom4B_3.pdf
16. H.T. Johansson, M. Heil, B. Löher, H. Simon, H. Törnqvist, Tech. rep. (2013), <http://repository.gsi.de/record/68045>
17. O.S. Kirsebom, M. Munch, H.O.U. Fynbo, in prep.
18. J. Kelley, J. Purcell, C. Sheu, Nuclear Physics A **968**, 71 (2017)
19. M. Munch, J.H. Jensen, O.S. Kirsebom, simX (2018)
20. J.F. Ziegler, M.D. Ziegler, J.P. Biersack, Nuclear Instruments and Methods in Physics Research B **268**, 1818 (2010)